Hindawi
Journal of Nanomaterials
Volume 2019, Article ID 6501923, 16 pages
https://doi.org/10.1155/2019/6501923

Research Article

Paper-Based Nanoplatforms for Multifunctional Applications

M. L. Matias,[1] D. Nunes,[1] A. Pimentel,[1] S. H. Ferreira,[1] R. Borda d'Agua,[1] M. P. Duarte,[2] E. Fortunato,[1] and R. Martins[1]

[1]*i3N/CENIMAT, Department of Materials Science, Faculty of Sciences and Technology, Universidade NOVA de Lisboa, Campus de Caparica, 2829-516 Caparica, Portugal*
[2]*MEtRICs, Department of Science and Technology of Biomass, Faculty of Sciences and Technology, Universidade NOVA de Lisboa, Campus de Caparica, 2829-516 Caparica, Portugal*

Correspondence should be addressed to D. Nunes; danielasilvanunes@gmail.com and R. Martins; rm@uninova.pt

Received 24 October 2018; Revised 3 February 2019; Accepted 12 February 2019; Published 4 April 2019

Academic Editor: Mohamed Bououdina

In this work, zinc oxide (ZnO) and titanium dioxide (TiO_2) nanostructures were grown on different cellulose paper substrates, namely, Whatman, office, and commercial hospital papers, using a hydrothermal method assisted by microwave irradiation. Pure ZnO and TiO_2 nanostructures were synthesized; however, the growth of TiO_2 above ZnO was also investigated to produce a uniform heterostructure. Continuous ZnO nanorod arrays were grown on Whatman and hospital papers; however, on office paper, the formation of nanoplates originating nanoflower structures could be observed. TiO_2 nanoparticles homogeneously covered all the substrates, in some conditions forming uniform TiO_2 films. Structural characterization was carried out by scanning electron microscopy (SEM) coupled with energy-dispersive X-ray spectroscopy (EDS), X-ray diffraction (XRD), and Raman spectroscopy. The optical characterization of all the materials was carried out. The produced materials were investigated for multifunctional applications, like photocatalyst agents, bacterial inactivators, and ultraviolet (UV) sensors. To evaluate the photocatalytic activity under UV and solar radiations, rhodamine B was the model-test contaminant indicator and the best photocatalytic activity was achieved with Whatman paper. Hospital paper with TiO_2 nanoparticles showed significant antibacterial properties against *Staphylococcus aureus*. ZnO-based UV sensors demonstrated a responsivity of 0.61 μA W^{-1}.

1. Introduction

Zinc oxide is an *n*-type semiconductor with a direct wide bandgap of 3.37 eV, and it has a large free exciton energy of around 60 meV (at room temperature) [1]. ZnO is used in a variety of applications, for instance, in thin film transistors [2], solar cells [3], UV/ozone, and glucose sensors [1, 4]; as a photocatalytic agent [5, 6]; and as an antibacterial and antifungal agent [7]. It has three polymorphs: wurtzite, rock salt, and zincblende structures; nevertheless at room temperature, the stable phase of ZnO is the hexagonal wurtzite [8]. The ZnO polar facets possess different chemical and physical properties from those presented by nonpolar facets, where the polar O terminated facet presents a slightly different electronic structure [9]. These characteristics are responsible for the vast different properties presented by ZnO, such as piezoelectricity and spontaneous polarization, being a key factor in crystal growth and in defect generation [9]. Indeed, ZnO's chemical and physical properties are highly influenced by its size, shape, morphology, and crystallinity, as well as the solvents and precursors used to achieve the desired nanostructure [10, 11].

Titanium dioxide is also an *n*-type semiconductor like ZnO, and its field of application ranges from sensors to solar cells [12–14]. Presently, this material is largely used as a photocatalyst [15–17]. Among the different structure phases that it might take, the most common ones are amorphous or the three crystalline phases: rutile, anatase (both tetragonal), and brookite (orthorhombic) [18]. TiO_2 is also a wide energy bandgap material, typically displaying optical bandgaps of 3.0 and 3.2 eV for rutile and anatase, respectively, and varying from 3.13 to 3.40 eV for brookite [18, 19]. Both metal

oxides are environmentally friendly, earth abundant, chemically stable, low-cost, nontoxic, and compatible with wet-chemical synthesis routes [20–23].

For both materials above described, there are several reports describing the use of hydrothermal/solvothermal synthesis to produce them [24–27], while more recently assisted process methods by microwave irradiation have been deeply exploited [28–30]. The main advantages of using the microwave technique to produce nanostructures are its reduced costs, low temperature, short reaction time, high reaction selectivity, low energy consumption, and homogeneous volumetric heating [31, 32]. Another characteristic of the microwave method is its high reaction rates, due to its ability to instantaneously localize heat into the material [33].

Among the substrates used, it has been previously reported that cellulose is compatible with wet-chemical synthesis routes [1, 12]. Moreover, this material is known as being the most abundant biopolymer on Earth, flexible, inexpensive, and recyclable, among other advantages. All these characteristics make this material highly attractive for nanoelectronics, sensors, photocatalysis, and antibacterial applications [1, 34]. Apart from that, recently the tendency towards the development of multifunctional devices with inexpensive substrates like paper has become the center of several scientific researches [35].

As far as it is concerned, photocatalysis is the acceleration of chemical reactions by photocatalysts which include semiconductors like TiO_2 and ZnO [36]. When these semiconductors absorb photon energy greater than their bandgap, the electrons from the valence band are excited to the conduction band and an electron-hole pair is created [37]. The electron-hole pair is a strong redox system [38], and in the presence of an absorbed compound in the photocatalyst surface, it can reduce and/or oxidize the compound [38–40]. As a result, the electrons will reduce oxygen on semiconductor surfaces, generating superoxide radicals and hydroperoxide radicals (•OHH) upon further reaction with H^+. The holes will oxidize OH^- and water molecules at the surface producing hydroxyl radicals (•OH) [28, 37, 38]. These superoxide ions, hydroxyl radicals, and hydroperoxide radicals will then interact with the dye and originate a range of intermediates to finally decompose the organic/inorganic compounds [29, 40].

The mechanism observed for UV sensing is similar to photocatalysis. The semiconductor photoconductivity relies on the electrical conductivity changes under irradiation. The photodetection is also governed by a hole-trapping mechanism based on the adsorption/desorption of chemisorbed oxygen molecules at the surface [41]. The antibacterial activity of TiO_2 and ZnO has also been investigated [7, 42]. Several studies suggest that these materials interact with the outer membrane of bacteria damaging the cell wall with the subsequent death of bacteria [28, 43].

In the present study, ZnO and TiO_2 nanostructures, together with ZnO/TiO_2 heterostructures, were grown on Whatman, office, and hospital paper-based substrates, under microwave irradiation at low temperature (80°C). To the best of the author's knowledge, ZnO and TiO_2 nanostructures as well as ZnO/TiO_2 heterostructures grown on various kinds of paper substrates to produce functionalized papers have never been reported before. It is worth emphasizing the novelty of synthesizing TiO_2 nanostructures using oxalic acid under microwave irradiation with fast synthesis time and the differences on ZnO structures regarding the use of each paper-based substrate. These materials were used as photocatalysts; nevertheless, they were also tested as UV sensors and antimicrobial agents originating multifunctional materials. The structural characterization of the materials has been carried out by scanning electron microscopy coupled with an EDS detector, Raman spectroscopy, and X-ray diffraction. The optical characterization has been also carried out for all materials processed in this study.

2. Experimental Procedure

2.1. ZnO and TiO_2 Synthesis. The ZnO and TiO_2 nanostructures have been produced using a hydrothermal synthesis assisted by microwave irradiation. Three different types of papers have been used, i.e., Whatman grade 2, office paper from INAPA Tecno SuperSpeed, and commercial hospital paper coming in a coach roll. For the uniform growth of ZnO nanostructures, a seed layer of ZnO had to be previously deposited on paper substrates [1], while for TiO_2 no previous treatment on the paper's surface has been carried out [12]. The ZnO seed layer was deposited by radio frequency (RF) sputtering with Argon (Ar), at room temperature [1]. A ceramic oxide target of ZnO with a purity of 99.99% was used for the deposition. For the depositions, the chamber was evacuated to a base pressure of 10^{-6} mbar. A shutter between the substrate and the target enabled the protection of the targets from cross-contamination. For the deposition of the ZnO seed layer, a power of 50 W and a deposition pressure of 4×10^{-3} mbar were used. The distance between the target and the substrate was fixed at 15 cm. The deposition was carried out for 90 minutes allowing the formation of ~200 nm ZnO layer. Prior to microwave synthesis, the ZnO seed layer had a subsequent UV exposure treatment (Novascan PSD UV-Ozone system) of 5 min to remove surface contaminants and to obtain a more polar surface of the ZnO seed layer that will improve the growth of the ZnO nanostructures [1]. The ZnO aqueous solution was composed of 25 mM zinc nitrate hexahydrate ($Zn(NO_3)_2{\cdot}6H_2O$; 98%, CAS: 10196-18-6) and 25 mM hexamethylenetetramine ($(C_6H_{12}N_4)_2$; 99%, CAS: 100-97-0) both from Acros Organics [1]. For TiO_2 NPs, the titanium(IV) isopropoxide ($Ti[OCH(CH_3)_2]_4$, TTIP) used was from Sigma-Aldrich (97%), CAS: 546-68-9. In a typical synthesis, 50 mL of deionized water is mixed with 10 mL of oxalic acid dihydrate ($C_2H_2O_4{\cdot}2H_2O$, CAS 6153-56-6, Merck Millipore). The molar concentration of acid was fixed 1 M; nevertheless, to produce the heterostructure, the molar concentration of 25 mM was also tested. Moreover, also in the case of the ZnO/TiO_2 heterostructure, the synthesis with no acid was investigated (60 mL H_2O). For both ZnO and TiO_2, solution volumes of 20 mL were transferred into capped quartz vessels of 35 mL, which were kept sealed by the constraining surrounding pressure. Paper pieces of $20.0 \times 20.0\ mm^2$ were previously cut and placed at an angle against the microwave vessel. In the case of ZnO, the seed

layer was facing down [31]. Temperature, power and maximum pressure of the microwave (CEM Focused Microwave Synthesis System Discover SP) were kept, respectively, at 80°C and 100 W for all materials. The microwave pressure was set to 150 Psi for TiO_2 and 300 Psi for ZnO nanostructures. The synthesis time was 15 min for ZnO and 15 min or 30 min for TiO_2 depending on the application selected. For the heterostructure, ZnO and TiO_2 microwave synthesis time was maintained at 15 min. After each synthesis process, the paper substrates were cleaned with deionized water and left drying overnight at room temperature.

2.2. Characterization Techniques. Surface SEM observations were carried out using a Carl Zeiss AURIGA CrossBeam FIB-SEM workstation and equipped for energy-dispersive X-ray spectroscopy (EDS) measurements. The dimensions of the nanostructures have been determined from SEM micrographs using the ImageJ [44] software and considering 30 distinct structures for each measurement. Micro-Raman spectroscopy experiments were carried out with inVia Qontor Confocal Raman Microscope from Renishaw, equipped with a 150 mW He–Ne laser operating at 532 nm.

XRD measurements were carried out in an X'Pert PRO PANalytical powder (X'Pert diffractomer using Cu Kα line radiation ($\lambda = 1.540598\,\AA$). Diffraction patterns were recorded from 20° to 70° (detector angle 2θ) with a step of 0.0330° in a Bragg-Brentano configuration. The simulated brookite corresponds to ICDD file No. 01-076-1937, the simulated rutile to ICSD file No. 96-900-4143, and the simulated anatase to ICSD: 082084 with $a = b = 3.7830\,\AA$ and $c = 9.4970\,\AA$. The simulated zinc oxide corresponds to ICSD file No. 00-036-145.

Room temperature diffuse reflectance measurements to obtain the optical bandgap were performed using a Perkin Elmer lambda 950 UV/VIS/NIR spectrophotometer with a diffuse reflectance module (150 mm diameter integrating sphere, internally coated with Spectralon). The calibration of the system was achieved by using a standard reflector sample (reflectance, $R = 1.00$, from Spectralon disk). The reflectance (R) was obtained from 250 to 800 nm.

2.3. Photocatalytic Activity. The photocatalytic activities of the ZnO and TiO_2 nanostructures as well as the ZnO/TiO_2 heterostructure were evaluated at room temperature considering the degradation of rhodamine B (RhB) from Sigma-Aldrich under a solar light–simulating source and UV radiation. All the experiments were considered according to the International Standard ISO 10678. The paper-based materials were placed at the bottom of the reaction recipient, and for each experiment, 50 mL of the rhodamine B solution (5 mg/L) was stirred for 30 min in the dark to establish absorption–desorption equilibrium. For the solar light exposure, a LED solar simulator LSH-7320 (AM 1.5 spectrum) was used at room temperature with an intensity of 100 mW/cm^2. For the UV exposure, a mercury lamp model HNSL from Osram Puritec was used with a power of 95 W. Absorption spectra were recorded using a PerkinElmer lambda 950 UV/VIS/NIR spectrophotometer with different time intervals up to a total of 21 h for solar radiation and 15 h for UV exposure.

2.4. UV Sensing. The synthesized ZnO nanostructures were characterized as a UV sensor on paper substrates with a potentiostat model 600, from Gamry Instruments, in a chronoamperometry configuration, with the application of a continued +10 V voltage. For interdigital electrical contacts, a carbon resistive ink was screen-printed (mesh 120 T). The produced materials were subjected to irradiation with an ultraviolet lamp, UVM-28 EL Series UV Lamp, with an intensity of 8 W at a wavelength of 302 nm. The experiments were performed with UV light irradiation for 3 min followed by 3 min in off state during 4 cycles. The ZnO nanorods grown on Whatman paper were the only condition that demonstrated a consistent UV sensing behavior, so the results of other materials were not presented in this study.

2.5. Determination of Antibacterial Activity. The antibacterial activity of hospital paper with TiO_2 nanoparticles synthesized for 15 min (1 M) was evaluated against *Staphylococcus aureus* ATCC6538 by the absorption method according to ISO 20743:2013(E), 2013, standards (International Standard ISO 20743:2013(E). Textiles—Determination of Antibacterial Activity of Textile Products. Second Edition, 2013) [45]. The materials were cut with a CO_2 laser (Universal Laser Systems VLS 3.5) in circles with a diameter of 3.5 cm on paper with and without (control) TiO_2 nanoparticles and exposed to UV radiation for 30 min on both sides. Then, bacterial suspension was directly inoculated into samples of control and samples of paper with TiO_2 nanoparticles. The antibacterial activity was evaluated quantitatively by comparing the number of colony-forming units (CFU) on the surface of paper with TiO_2 nanoparticles and control paper after incubating at 37°C for 18 h.

3. Results and Discussion

ZnO and TiO_2 nanostructures as well as ZnO/TiO_2 heterostructures were successfully synthesized under microwave irradiation using cellulose-based substrates at low temperatures and fast synthesis times. The distinct substrates were selected due to their specific application targets. Whatman is a chromatography paper, being composed by highly pure cellulose, without any additives. This paper was thought for photocatalysis and UV sensing applications. Office was also selected for photocatalysis, but in terms of high abundancy and low cost to obtain a disposable photocatalytic paper. At last, hospital paper was selected for the antibacterial activity experiments in a way to avoid growth and proliferation of microorganisms commonly found in the hospital environment, and besides it is a disposable paper. This latter paper was also tested for photocatalysis. The produced nanostructures, as well as the ZnO/TiO_2 heterostructure, substrates, and final devices were systematically investigated, and multifunctional materials were produced.

3.1. Structural Characterization. Figure 1 shows the ZnO nanostructures synthesized under microwave irradiation and using Whatman (a), office (b), and hospital (c) papers

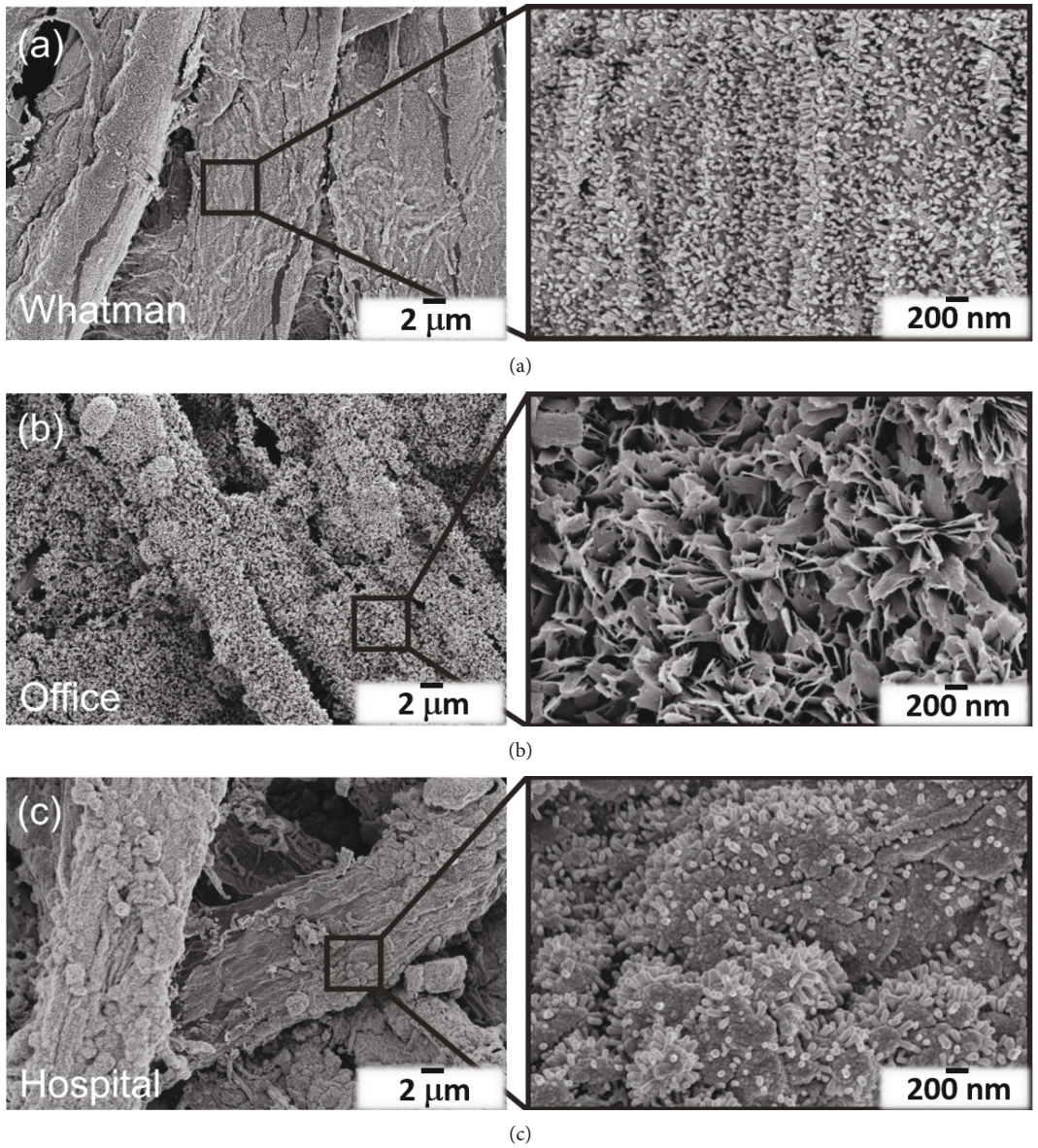

Figure 1: ZnO nanostructures grown on (a) Whatman, (b) office, and (c) hospital papers. The insets magnify the nanostructures synthesized.

as substrates. Microwave irradiation resulted in uniformly covered substrates forming continuous ZnO nanostructured arrays with two distinct film characteristics. Whatman and hospital papers resulted in continuous ZnO nanorod arrays, while on office paper nanoplates originating flower-like structures have been observed. An analogous study had previously demonstrated the growth of ZnO nanorod arrays on Whatman paper [1]. The discrepancies observed on these three types of papers are thought to be related to the impurities present on the substrates, i.e., calcium carbonate ($CaCO_3$). EDS analyses were carried out on the pristine paper substrates, and the results are presented in Figure S1. Both office and hospital papers revealed the presence of Ca appearing as agglomerates. Some minimal traces of Al and Si were also observed on hospital paper. Whatman paper, on the other hand, is highly pure, presenting just C and O (Table S1).

Some studies demonstrated the effect of adding calcium carbonate and ZnO, as well as the interaction between these materials [46, 47]. In Ref. [48], it has been demonstrated that $CaCO_3$ effectively changes the physical properties of ZnO. Moreover, Tian et al. [49] showed that the ZnO synthesis with sodium citrate originates plates instead of nanorods, in a way that citrate ions strongly bind to the Zn atoms on the (002) surfaces resulting in hexagonal ZnO nanoplates. A similar effect is expected to have occurred with ZnO and the calcium carbonate present on office paper, in which the ZnO-rod like structure growth along the ⟨001⟩ orientation was hindered, producing plates. Comparing both office and hospital papers, where calcium carbonate was detected (Figure S1 and Table S1), the presence of this element in higher amounts in office paper has been observed. In the case of Whatman paper, the ZnO average nanorod lengths were 160.7 ± 3.4 nm, while in the case of

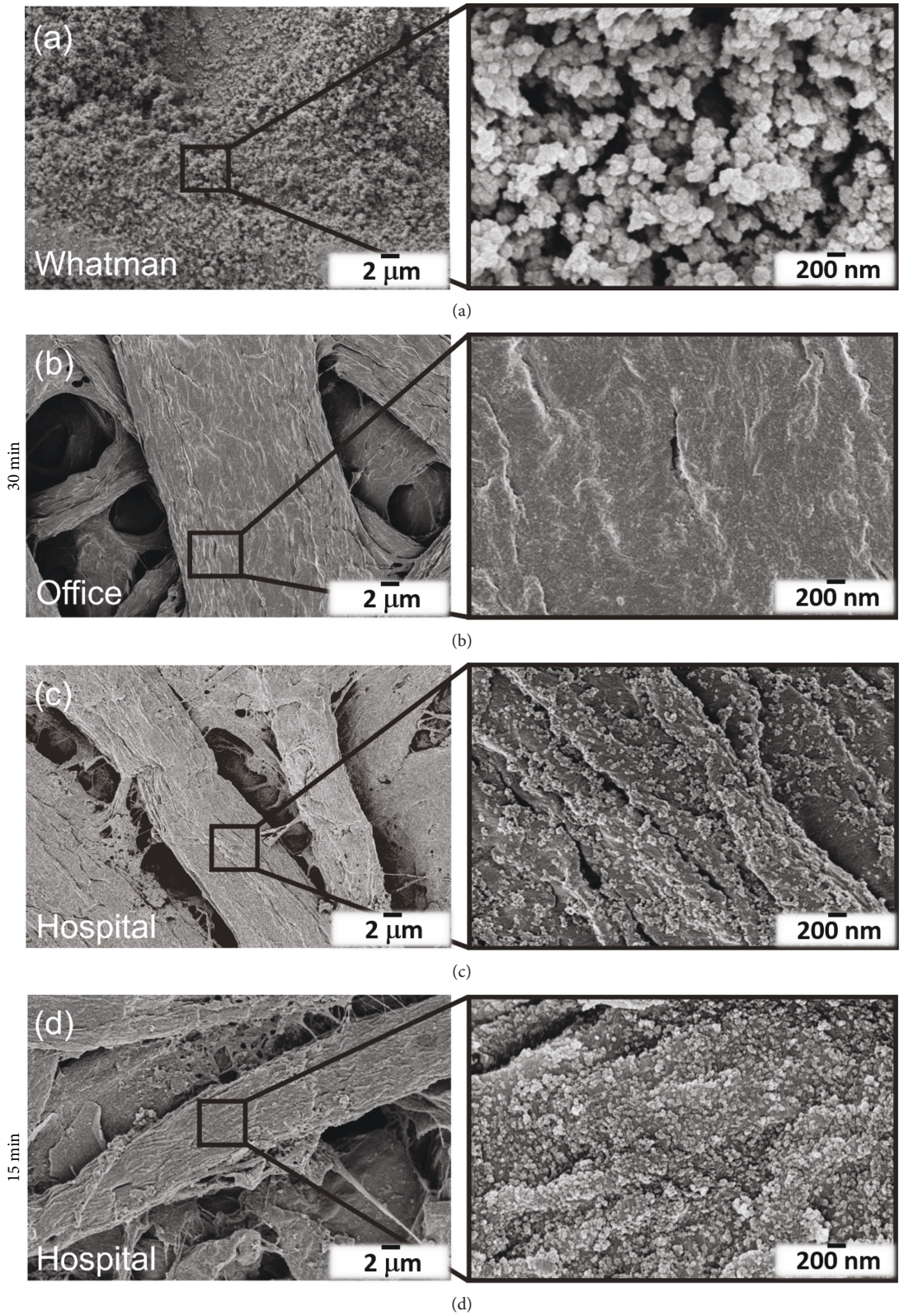

FIGURE 2: TiO_2 nanostructures grown on (a) Whatman, (b) office, and (c) hospital papers at 30 min synthesis time. (d) TiO_2 nanostructures synthesized at 15 min. The insets magnify the nanostructures formed after microwave synthesis.

hospital paper, the value was 128.6 ± 4.3 nm. The length of the plates' structures observed on office paper could not be certainly determined.

Figure 2 depicts the TiO_2 nanoparticles and films synthesized under microwave irradiation and using Whatman (a), office (b), and hospital (c) papers as substrates. In the case

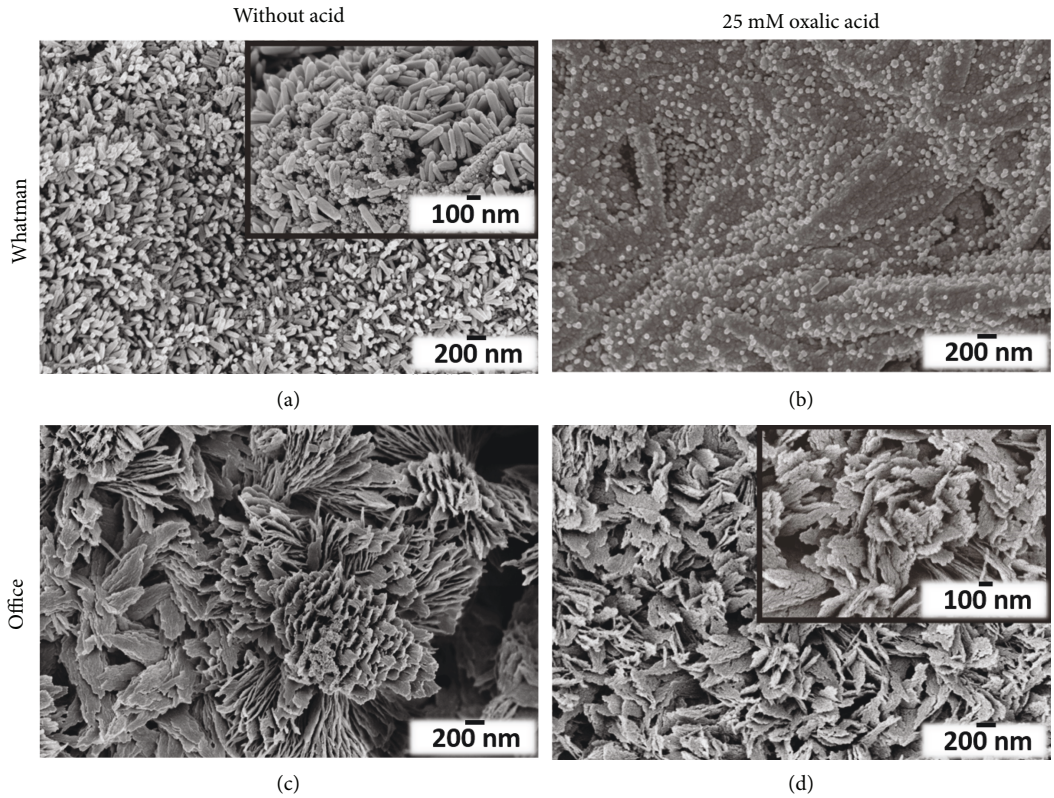

Figure 3: ZnO/TiO_2 heterostructures grown on Whatman paper having TiO_2 synthesized (a) without acid and (b) with 25 mM of oxalic acid, and office paper (c) without acid and (d) with 25 mM of oxalic acid. The ZnO and TiO_2 nanostructures were both synthesized considering 15 min of synthesis time. The inset in (a) magnifies the heterostructure, while the inset in (d) evidences the surface modification with oxalic acid.

of hospital substrate, two synthesis times were investigated, that is, 15 and 30 min. As observed for ZnO materials, microwave irradiation also resulted in uniformly covered substrates without any seed layer. Individual nanostructured particles with an undefined structure have covered the majority of the paper's surface and in some cases forming larger agglomerates. In some conditions, the nanoparticles grew forming films on the substrate surfaces. The film synthesized on Whatman paper was composed by dense agglomerates of TiO_2 nanoparticles, while a thinner film could be seen on office paper. On hospital paper, these individual nanoparticles were randomly distributed, in some cases appearing as agglomerates, but in smaller amounts when compared to the ones observed on Whatman paper. The average diameter of the nanoparticles synthesized on Whatman paper was 147.6 ± 26.6 nm. In the case of the nanoparticles formed on hospital paper with 15 min of microwave synthesis, the average size was determined to be 29.5 ± 1.9 nm, while in the case of 30 min synthesis, the average size was 305 ± 5.5 nm. The nanoparticles formed on the office paper substrate could not be easily distinguished and have not been measured.

Comparing both conditions investigated on hospital paper, it has been observed that with a 30 min synthesis, slightly larger nanoparticles were formed, and the agglomerates became greater in size (not so many isolated nanoparticles were detected). And for that reason, the 15 min synthesis condition was selected for the antibacterial activity experiments, while that at 30 min was used for photocatalysis. Moreover, smaller nanoparticles could more easily penetrate the permeable membrane of bacteria [45]. The heterogeneities and roughness of the cellulose fibers did not allow the determination of thicknesses from the materials produced.

EDS analyses were carried out in both ZnO and TiO_2 materials confirming the well-distributed materials along the substrates (Figure S2). EDS point analyses were also performed to provide the relative quantities (at.%) of each element (Table S1). As previously observed in an analogous study, all the TiO_2 films were grown on both sides of the cellulose-based substrates [12].

The ZnO/TiO_2 heterostructures were also successfully produced under microwave irradiation using paper-based substrates. Nevertheless, the ZnO/TiO_2 heterostructure on hospital paper-based materials has not been investigated, since the paper is easily folded after synthesis, making it difficult to work with, especially after two individual microwave syntheses. To prevent the chemical attack of ZnO, the oxalic acid concentration was expressively decreased (1 M to 25 mM) and the TiO_2 synthesis was performed without any acid. Figure 3 shows the ZnO/TiO_2 heterostructures grown on Whatman and office papers with (25 mM) or without oxalic acid. The effect of acid-based TiO_2 syntheses was evident on ZnO nanostructures present on both substrates.

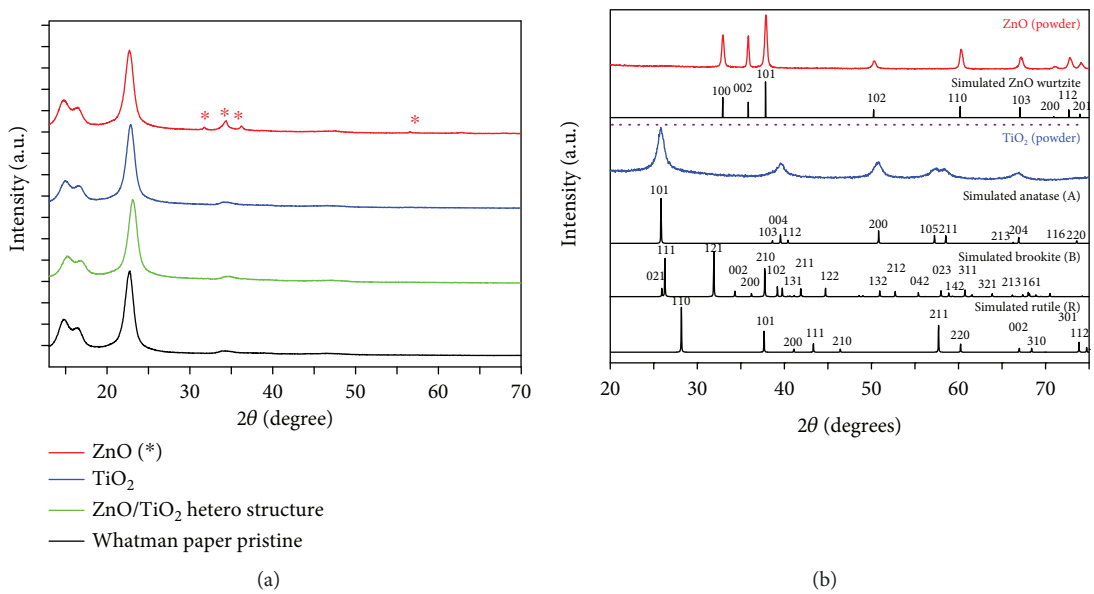

Figure 4: (a) XRD diffractograms of ZnO and TiO_2 (1 M, 30 min) nanostructures grown on Whatman paper substrate. The ZnO/TiO_2 (25 mM) heterostructure-based material is also presented together with the Whatman pristine paper. The ZnO peaks are identified with asterisks (*). (b) ZnO and TiO_2 powder produced during microwave synthesis. The simulated ZnO wurtzite, TiO_2 anatase, rutile, and brookite structures are presented.

In Figure 3(b), the etching of the ZnO nanorods is clear after a 15 min TiO_2 microwave synthesis. The average ZnO nanorod lengths decreased to 95.6 ± 2.0 nm. The ZnO acid chemical etching has been reported previously [50, 51]. Nevertheless, oxalic acid was expected to have low impact on the ZnO nanostructure, since the use of oxalic acid to synthesize ZnO has been reported [52, 53]. On office paper, the etching effect was also observed with deterioration of the plate's surface and appearance of laminar structures together with occurrence of holes (see inset on Figure 3(d)). Regarding the presence of TiO_2, the individual nanoparticles grew surrounding the ZnO nanorods on Whatman paper, as it can be seen on the Figure 3(a) inset. The presence of TiO_2 agglomerates was also detected in some conditions. Nevertheless, uniformly TiO_2 films covered all the substrates as previously observed in Figure 2 and as attested by EDS analyses (Figure S2). In the case of office paper, the individual nanoparticles were not discernible; however, a thin film is believed to have covered the ZnO nanostructures, such as that presented in Figure 2(b).

The EDS analyses of the ZnO/TiO_2 heterostructure formed on Whatman paper are presented in Figure S2 (m), and the homogeneous distribution of Zn along the substrate could be observed (Figure S2 (p)), and Ti in a lower extent. TiO_2 agglomerates were clearly identified in Figure S2 (q).

X-ray diffraction and Raman spectroscopy measurements were carried out for the ZnO and TiO_2 nanostructures but also for the heterostructure. The materials grown on Whatman paper were the only measurements presented, since office and hospital papers displayed XRD peaks [54] and intense fluorescence on Raman measurements coming from the calcium carbonate [55, 56]. Nevertheless, a substantial contribution from the Whatman substrate was also observed on both techniques, hindering the ZnO or TiO_2 signals (Figure S4). Moreover, the greater contribution coming from the substrates is also associated to the reduced thickness of the metal oxide-based films/arrays produced, especially in the case of TiO_2. The XRD results (see Figure 4(a)) show that the characteristic peaks of native cellulosic fibers $(1\bar{1}0)$, (110), (200), and (004) at $2\theta = 14.9°$, $2\theta = 16.6°$, $2\theta = 22.7°$, and $2\theta = 35°$, are, respectively, in agreement with the literature [1]. No impurities or other crystallographic phases were detected. In Figure 4(a), the growth of ZnO nanostructures on cellulose-based substrates could be confirmed. The observed hexagonal wurtzite ZnO peaks were identified as the crystallographic planes (100), (002), (101), and (110). An analogous study also demonstrated the formation of pure ZnO on Whatman paper grown under microwave irradiation [1]. In, the case of TiO_2, the paper signal totally obscured its signal. The XRD measurements of the ZnO/TiO_2 heterostructure were also inconclusive, since TiO_2 could not be identified and the reduced size of ZnO due to chemical etching may have contributed to the lack of the ZnO signal coming from the material. As an alternative for TiO_2 phase identification, the powder formed during the microwave synthesis has been analyzed. ZnO in the form of powder is also presented for comparison (Figure 4(b)). XRD results confirmed that the produced material is fully assigned to the hexagonal wurtzite ZnO crystalline structure. In the case of TiO_2, all peaks in the experimental diffractograms could be assigned to the anatase phase. No peaks associated to impurities such as $Ti(OH)_4$ were detected, and all the peaks suggest that the materials are well crystallized. Several studies reported the formation of anatase TiO_2 under microwave irradiation [57–59]; nevertheless, to the best of the authors' knowledge, the production of anatase TiO_2 nanostructures

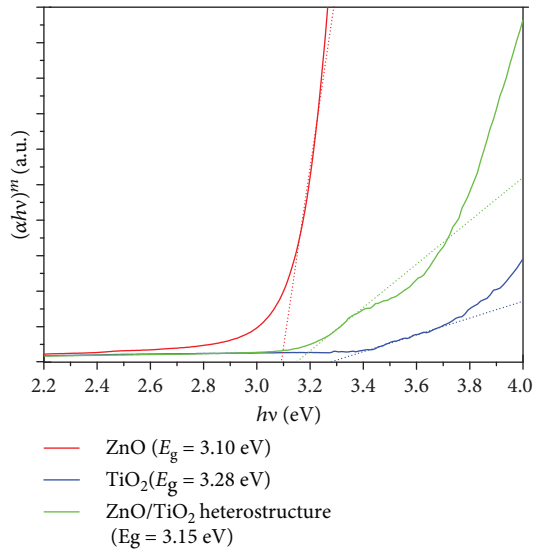

FIGURE 5: $(\alpha h\nu)^m$ versus photon energy $h\nu$. The optical bandgap measurements were carried out for the ZnO (15 min) and TiO_2 nanostructures (1 M, 30 min), as well as the ZnO/TiO_2 heterostructure (25 mM). All materials have been grown on Whatman paper.

grown on paper substrates under microwave irradiation has never been reported before.

The effect of oxalic acid on TiO_2 crystal growth has been reported by Fahmi et al. [60]. It has been stated that the growth of rutile is favored, because oxalic acid binds more strongly to anatase. Moreover, it has been suggested that oxalic acid undergoes dissociation (splitting of both H atoms), and the resulting oxalate ion, $C_2O_4^{2-}$, is bonded through the oxygen atom to neighboring Ti atoms [61]. In the present study, all the microwave syntheses led to the formation of pure TiO_2 anatase instead of rutile. This behavior may be resultant of microwave synthesis and its characteristics, such as microwave coupling efficiency to the solvent and heating rate, among others.

3.2. Optical Characterization. The optical bandgap values for TiO_2 and ZnO nanostructures together with the ZnO/TiO_2 heterostructure are presented in Figure 5. Reflectance data was acquired to evaluate the optical bandgap through the Tauc plot. Based on Equation (1), it is possible to determine the optical bandgap (E_g) by plotting $(ahv)^m$ against $h\nu$ and through the extrapolation of the linear part with 0:

$$(\alpha h\nu)^m = A\left(h\nu - E_g\right), \quad (1)$$

where α is the linear absorption coefficient of the material, $h\nu$ is the photon energy, A is a proportionality constant, and m is a constant exponent which determines the type of optical transitions ($m = 2$ is for direct allowed transition and $m = 1/2$ for indirect transitions) [12]. The bandgaps of the nanostructures on hospital and office papers were not presented due to the high influence (high reflectance peaks) coming from the paper substrates. For ZnO nanorods, a direct optical bandgap was considered, while for TiO_2, it has been assumed that the nanostructures are from the anatase phase as observed in XRD measurements (Figure 4(b)) and for that case with an indirect optical bandgap.

The bandgaps estimated were 3.10 and 3.28 eV for ZnO and TiO_2 nanostructures, respectively. These values are in agreement with the ones reported in the literature, that is, between 3.1 and 3.3 eV for ZnO [62, 63] and around 3.2 eV for anatase TiO_2 [31, 64]. The ZnO bandgap value is in agreement with an analogous study, in which ZnO nanorods were fabricated on Whatman paper [1]. For the ZnO/TiO_2 heterostructure, the presence of two phases can be seen. Thus, the bandgap value is expected to be a contribution of both nanostructures (TiO_2 and ZnO).

3.3. Photocatalytic Activity. ZnO and TiO_2 have been largely used in photocatalysis, in which the latter continues to be one of the most widely embraced photocatalysts nowadays [12, 31, 65]. ZnO and TiO_2 are wide bandgap materials, which makes them active under UV light irradiation, and thus it is expectable that both materials have higher photocatalytic activity under UV than under solar radiation [31].

Nevertheless, in terms of pollutant degradation with UV irradiation, this procedure is extremely limited, and the use of the complete solar spectrum is highly desired. In the present study, both ZnO and TiO_2 have been exposed to UV and solar radiation; however, ZnO and the ZnO/TiO_2 materials did not show any significant RhB degradation (results not shown) under solar radiation, and for that matter, just TiO_2 materials are presented in Figure 6.

The photocatalytic activity of TiO_2 grown on Whatman and hospital papers was evaluated through the degradation of rhodamine B under solar radiation, and the results are presented in Figure 6. The material grown on office paper did not reveal any RhB degradation under solar radiation, and it is expected to be due to the reduced thickness of the film produced (Figure 2(b)). The condition analyzed for the photocatalytic experiments was 1 M and 30 min, since dense/larger agglomerates of TiO_2 nanoparticles were produced (Figure 2). The maximum absorption peak of RhB is in accordance with the literature and in aqueous solution is located at 554 nm [66]. For both Whatman and hospital paper-based TiO_2 materials, it is clearly visible and previously stated in other studies that the RhB degradation is accompanied by a slight hypsochromic shift of absorption bands [67]. The TiO_2 Whatman-based material (Figure 6(a)) achieved a degradation value of 57% when compared to 50% of degradation observed in hospital-based material (Figure 6(b)), both after 21 h of solar light exposure. Thus, a comparable degradation behavior could be observed for both materials under solar radiation.

It has been proposed that under the exposure of solar light, RhB degradation results in N-deethylation and cleavage of chromophore with the final mineralization of the dye [12, 68].

The photocatalytic activity of ZnO and TiO_2 nanostructures, together with the ZnO/TiO_2 heterostructure, was also evaluated through the rhodamine B degradation efficiency under UV irradiation. In the case of ZnO nanostructures, the hospital paper resulted in smaller nanorods, which compromised its photocatalytic performance also under UV

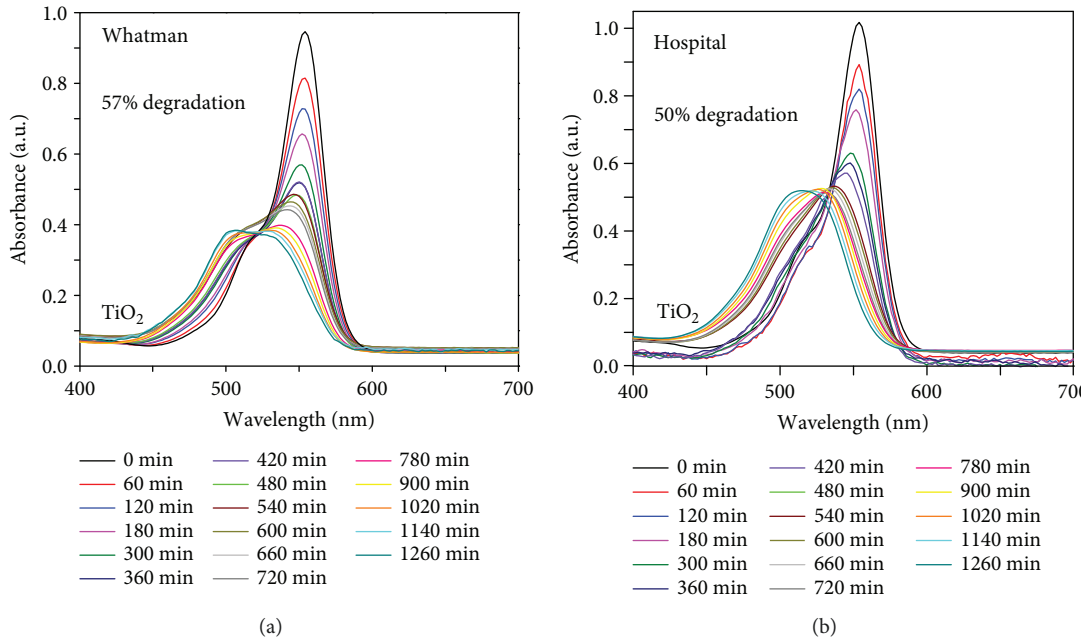

Figure 6: RhB absorbance spectra under simulated solar light radiation (led simulator with AM 1.5 Spectrum) up to 21 h for TiO_2 nanostructures grown on (a) Whatman and (b) hospital papers (1 M, 30 min synthesis time) at room temperature.

irradiation. In the case of TiO_2, as observed in solar radiation experiments, the office paper-based materials did not reveal significant photocatalytic activity under UV irradiation and the results have not been presented.

The photocatalytic activity of ZnO nanostructures grown on Whatman and office papers is presented in Figures 7(a) and 7(b), respectively. A RhB degradation of 40% and 51% was obtained at 15 h of UV exposure, for ZnO nanostructures grown on Whatman and office papers, respectively. The highest photocatalytic activity observed on office-based materials is expected to be related to the higher surface/volume ratio of the nanoplates forming the flower-like structure (Figure 1), which results in a higher density of active sites for surface reactions. Moreover, the morphology and the specific crystal facets play an important role in ZnO catalytic properties, since different crystal facets have different dangling bond configurations [69]. No contribution from different phases is expected on ZnO, since all materials are expected to have the hexagonal wurtzite ZnO structure. The optical bandgap could not be determined for most of the paper-based substrates, so no direct conclusion can be stated (Figure 5).

In the case of TiO_2, as investigated in solar radiation experiments, Whatman and hospital-based materials were also exposed to UV irradiation. Identical RhB degradation values to the solar radiation experiments were obtained under UV irradiation, i.e., 57% for the TiO_2 Whatman-based material and 50% for the hospital-based one. Nevertheless, a significant smaller exposure time was required (15 h instead of 21 h). Nevertheless, the higher photocatalysis under UV than under a solar simulating light source is expectable, since TiO_2 is a wide-bandgap semiconductor [12, 31].

The enhanced photocatalytic activity of TiO_2 is also related to the presence of the anatase phase. Anatase is largely used as photocatalyst, and it composes the commercial Degussa P25 catalyst. Anatase is considered a better photocatalyst than other TiO_2 polymorphs are, i.e., rutile and brookite. Nevertheless, the photocatalytic behavior of these TiO_2 polymorphs has been under intense debate over the years. One possible reason for anatase's better photocatalytic performance is its indirect bandgap that exhibits a longer lifetime of photoexcited electrons and holes when compared to the direct bandgap rutile and brookite [64].

In terms of active facets, the reactivity of the facets also differs; in anatase, the active facets are {111}>{001}>{100}>{101} [70], thus some contribution coming from them is expected. Regarding the size effect, the TiO_2 nanoparticles observed on Whatman paper were expressively larger than the ones on hospital paper. Moreover, a better and more dense coverage of the substrate was also observed on Whatman-based substrates with the formation of larger agglomerates (Figure 3). As a result, more catalysts are available during reaction, which could increase the absorbance of incident light and thus the generation of charge carriers [68].

The photocatalytic activity ZnO/TiO_2 heterostructures has also been investigated under UV irradiation. Both TiO_2 syntheses with and without acid have been tested. In Figure 7, the results of the ZnO/TiO_2 heterostructure having TiO_2 synthesized without acid on Whatman and office papers are presented. The combination of nanostructures was expected to improve the photocatalytic activity, decreasing the recombination of electron-hole pairs and increasing the lifetime of carriers. As a result, there should be an improvement in the interfacial charge transfer and thus in the redox reactions [71]. This, however, was not observed on Whatman (Figure 7(e)) and office paper-based materials (Figure 7(f)).

In fact, comparing the ZnO Whatman-based material to the ZnO/TiO_2 heterostructure, it can be observed that it

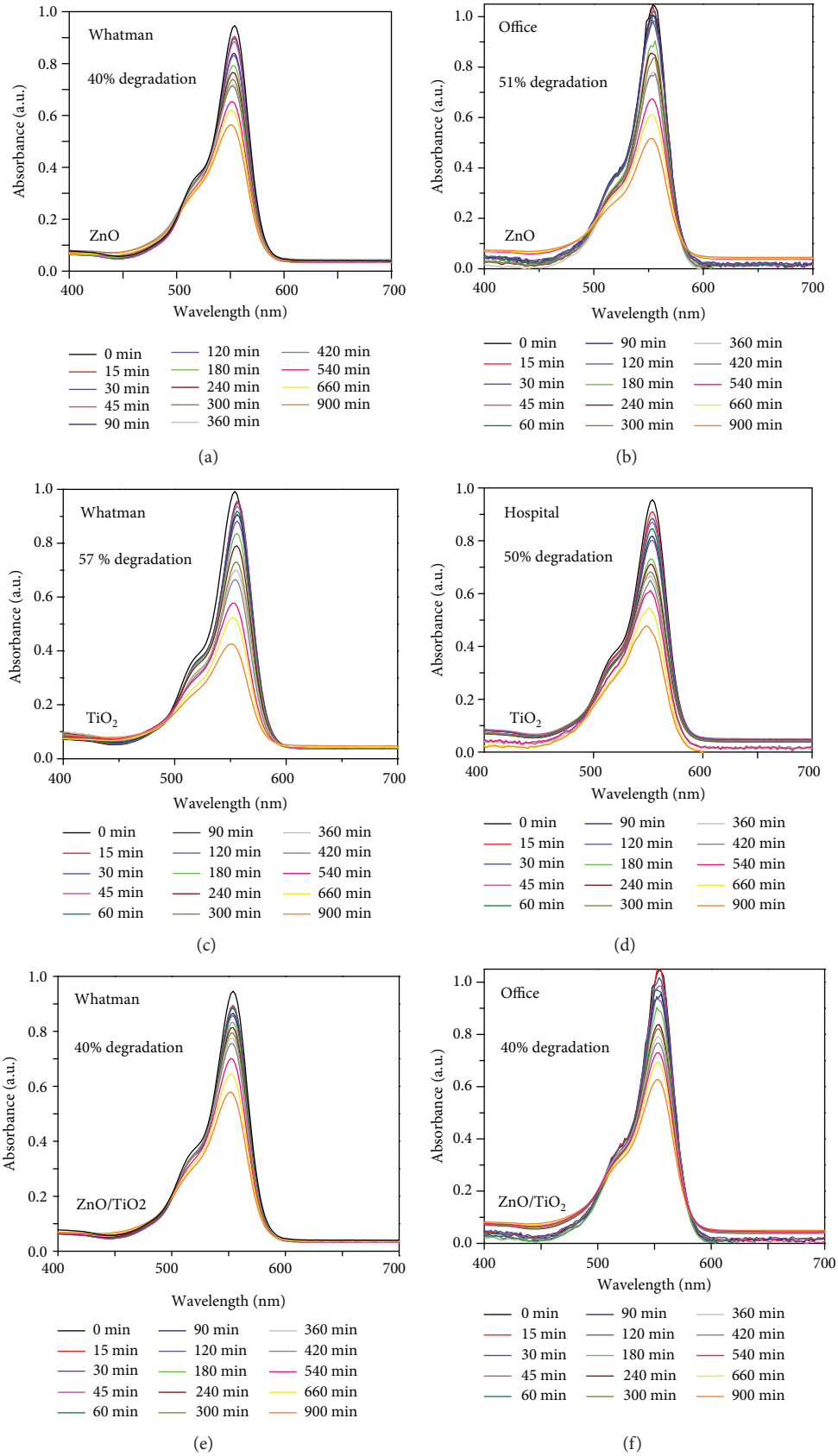

Figure 7: RhB absorbance spectra under UV light exposures up to 15 h for ZnO nanostructures on (a) Whatman and (b) office papers; TiO_2 nanostructures (1 M, 30 min) grown on (c) Whatman and (d) hospital papers; and ZnO/TiO_2 heterostructures synthesized (e) without acid on Whatman and on (f) office papers. The measurements were carried out at room temperature.

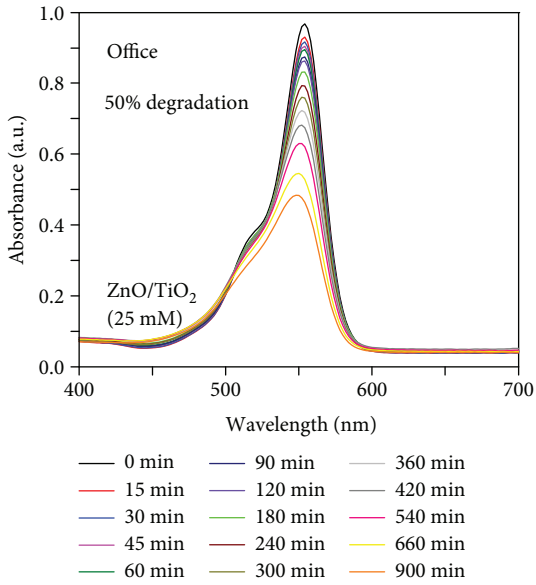

FIGURE 8: RhB absorbance spectra under UV light exposure at room temperature up to 15 h for the ZnO/TiO_2 heterostructure (25 mM, 15 min) grown on office paper.

achieved the same RhB degradation (40%) with equal UV exposure times. When compared to the ZnO material grown on office paper, an RhB degradation reduction to 40% was observed if compared to the 51% achieved by the pure material. In the case of the TiO_2 materials grown on Whatman paper, the RhB degradation reduction was more expressive (57% of pure TiO_2 to 40% of the heterostructure). These results indicate that the TiO_2 nanostructures (without acid) grown above ZnO could not effectively contribute to photocatalysis and in some extent interfere with the photocatalytic process. It is believed that the TiO_2 formed without acid has the anatase structure, as observed for the powder produced during heterostructure synthesis, with reduced size (see the broader peaks on Figure S4). However, an incomplete conversion of phase can be expected for synthesis without acid, which may have compromised the photocatalytic performance of TiO_2. Moreover, as reported in the literature, the acidic environment during the growth process of titanium dioxide nanoparticles is appropriate for the formation of well crystalline nanoparticles [72], and the lack of acid can result in amorphous materials [73].

The ZnO/TiO_2 heterostructure (25 mM) grown on office paper has also been investigated as photocatalyst. An RhB degradation of 50% was obtained (Figure 8), and in the previous case (without acid) it was 40% after 15 h of exposure time. The presence of acid even in smaller concentration can be responsible for the better TiO_2 performance and, when associated to the chemical etching of ZnO (structure modification), could have contributed to the overall enhanced photocatalytic activity. The holes and deterioration of the plate surface with laminar structures observed in Figure 3(d) are expected to have a higher surface area, and thus more active sites will have been available for the dye molecules to react with the catalyst [30].

The degradation ratio (C/C_0) vs. UV/solar light exposure time is presented in Figure 9, in which C is the absorbance of the RhB solution for each exposure time and C_0 is the initial solution absorbance [12]. A blank solution of rhodamine B was also exposed to solar/UV radiations. It has been observed that the blank solution was not influenced in both cases, and it can be concluded that the photocatalytic activity was only influenced by the catalyst. From Figure 9, it can be observed that under solar and UV radiations, the TiO_2 nanostructures grown on Whatman paper (1 M and 30 min synthesis time) had the highest photocatalytic activity among the materials investigated.

All these photocatalytic experiments open up to the production of smart photocatalytic papers capable of decomposing organic pollutants when light-activated, even under solar radiation. The idea is to produce one-use materials that are biocompatible, flexible and thus can be adapted to several surfaces, disposable, and can be easily recycled. Moreover, the approach developed in this study revealed to be clean, as no powder or extra processes have been used during photocatalysis, and environmentally friendly photocatalysts such as ZnO and TiO_2 have been employed.

3.4. UV Sensing. Both zinc oxide and TiO_2 are highly sensitive to adsorption and desorption of gases due to oxygen vacancies on the surface [74, 75]. Regarding the sensing mechanism, with no UV exposure (in the dark) and upon oxidation, the oxygen molecules adsorb to the surface of the semiconductors (ZnO or TiO_2) and accept free electrons leading to an electron reduction from the conduction band. As a result, the conductivity decreases. When the semiconductors are exposed to UV radiation, electron-hole pairs are generated when the incident photon energy is higher that their bandgap and holes migrate to the surface accelerated by a potential slope. This potential slope is produced by band bending, and the negatively charged absorbed oxygen molecules are discharged under electron-hole recombination. As a consequence, oxygen is desorbed from the surface and the conductivity of the semiconductor increases [76, 77]. In the present study, ZnO and TiO_2 nanostructures grown on Whatman, hospital, and office papers have been tested as UV sensors. The ZnO/TiO_2 heterostructures were not investigated as UV sensors. Regarding the used substrates, hospital and office paper made the production process of the sensors difficult due to the porosity of the cellulose fibers, higher roughness, and presence of impurities ($CaCO_3$). Whatman paper, on the other hand, has been previously reported as substrate for UV sensors and, in this study, was also used for such devices. TiO_2 grown on Whatman paper did not behave as an UV sensor, and the most likely reason is the lack of seed layer below the nanostructures that would produce a continuous and interrupt film, avoiding any current loss.

In the case of ZnO, the nanorod arrays grown on Whatman paper were successfully employed as UV sensors. The time-resolved photocurrent of ZnO nanorod paper UV sensor is presented in Figure 10.

In Figure 10, it is possible to observe that the photocurrent exponentially increased from 0.10 μA to 5.0 μA (bias voltage of +10 V) and then decreased to its original value in

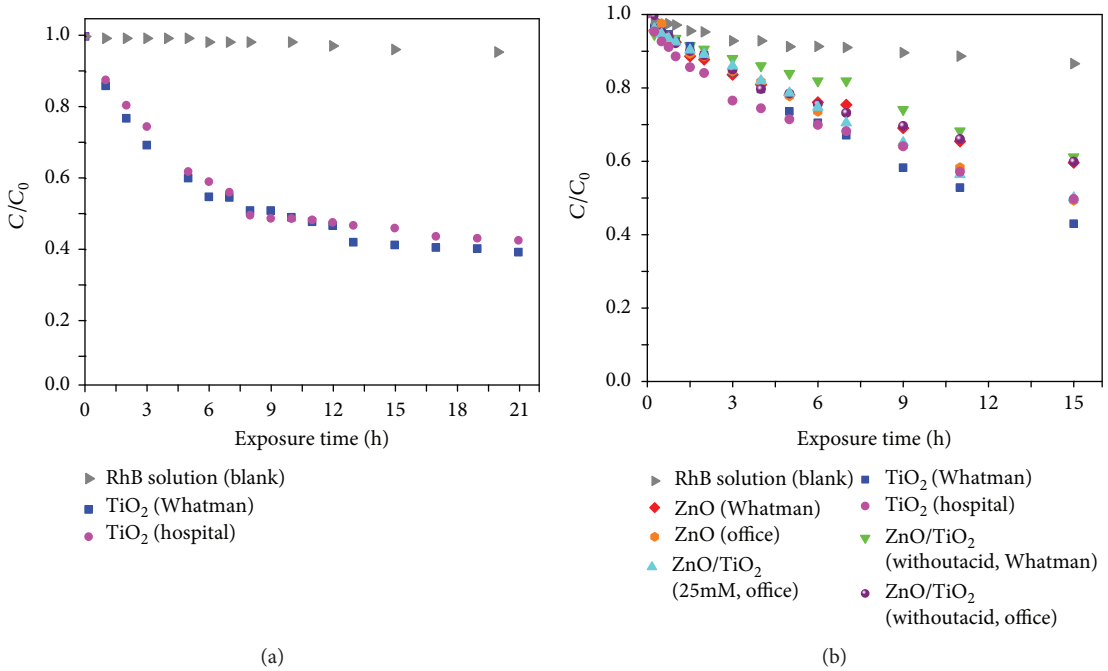

Figure 9: (a) RhB degradation ratio (C/C_0) vs. solar light exposure time and (b) RhB degradation ratio (C/C_0) vs. UV exposure time.

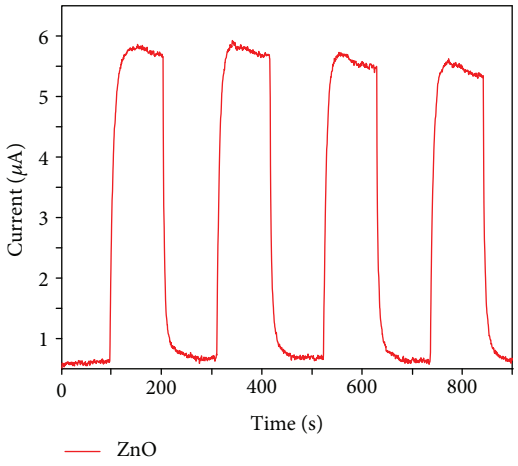

Figure 10: ZnO-based UV sensor (80°C, 15 min) grown on Whatman paper with carbon contacts impressed by screen-printing.

approximately 109 s after the UV radiation was turned off. The photocurrent of ZnO UV sensors was completely reproducible during several cycles of photocurrent switching. The responsivity was calculated according to the following equation [12]:

$$R = \frac{I_{\text{ph}} - I_{\text{dark}}}{P_{\text{UV}}}, \tag{2}$$

where I_{ph} is the UV sensor photocurrent, I_{dark} is the UV sensor dark current, and P_{UV} is the power of the UV source. Based on Equation (2), the obtained responsivity value was 0.61 μA/W. For the responsivity, the current value when the sensor reaches 95% of its stable value was taken into account [1]. This value is almost 2 times lower than the one obtained in [1] (1.19 μA/W); however, a lower temperature was used in the present study. According to the literature, higher temperatures lead to a better coverage of the substrate with nanorods as they become higher in length and well aligned. An increase in length leads to a higher aspect ratio of length to diameter which increases the sensitivity and responsivity [1].

3.5. Antibacterial Activity: Absorption Method. Metal oxide nanostructures have a lot of potential as antimicrobial agents, because of their capability and high selectivity, for instance, in biological and pharmaceutical applications [43]. Several studies suggest that the high antibacterial activity of TiO_2 nanoparticles, when photoactivated, is mainly due to the peroxidation of the polyunsaturated phospholipids of the lipid membrane. However, it has been reported that a UV light exposure with shorter wavelengths (UV-C and UV-B) leads to a faster and more efficient antimicrobial TiO_2 effect [28, 78]. In terms of the substrate, hospital papers coming as coach rolls are widely used nowadays, and thus this approach can contribute to avoid proliferation of bacteria, while maintaining the low cost and abundancy aspects of the material.

S. aureus are gram-positive abundant skin-colonizing bacteria and a very important cause of both nosocomial infections and community-associated skin infections [11]. The antibacterial activity of TiO_2 nanostructures grown on hospital paper (1 M, 15 min synthesis time) against this bacteria was quantitatively assessed accordingly to [7]

$$A = (\log C_T - \log C_0) - (\log T_T - \log T_0), \tag{3}$$

where A is the value of the antibacterial activity, $\log C_T$ and $\log T_T$ are the common logarithm of the average

number of CFU obtained with control (C) and nanoparticle-impregnated samples (T), respectively, immediately after inoculation (C_0 and T_0) and after the 18 h incubation (C_T and T_T). To evaluate the effectiveness of the assay on the materials, a classification is attributed, and if $2 \leq A < 3$, the antibacterial properties are significant, or if $A \geq 3$, they are strong [7, 45].

The results showed that after 18 h of incubation, the control paper supported the growth of *S aureus*. The obtained value for the antibacterial activity was 2.04. This value indicates significant TiO_2 antibacterial properties and means that, after inoculation and incubation, the logarithm of the number of bacteria in hospital paper functionalized with nanoparticles was 2.04 times lower than in control. The present results demonstrated that the investigated material has a satisfactory antibacterial activity, and with more investigation and development, these materials can be produced in large-scale and evolve into the hospital environment, maintaining their low-cost characteristics.

4. Conclusions

ZnO and TiO_2 nanostructures as well as ZnO/TiO_2 heterostructures were synthesized under microwave irradiation at a low temperature (80°C), using synthesis times up to 30 min. Low-cost Whatman, office, and hospital paper substrates were used. The synthesized materials were integrated on different applications, namely, photocatalysis, UV sensors, and antimicrobial agents. Microwave synthesis successfully covered the substrates with the nanostructures in all conditions studied. Significant differences in ZnO structure was observed, regarding the paper used. For TiO_2 synthesis, oxalic acid was used, and the materials produced had the anatase phase. The photocatalytic activity of the materials was assessed from rhodamine B degradation and the highest photocatalytic activity was obtained with pure TiO_2 nanostructures grown on Whatman paper. The presence of dense agglomerates forming thick TiO_2 film layers on Whatman paper as well as the ZnO nanoplates with high surface area on office paper have contributed to the degradation of the pollutant in photocatalysis experiments. A ZnO-based UV sensor was fabricated on Whatman paper, demonstrating good responsivity and reproducibility during more than four tested cycles. TiO_2 nanostructures grown on hospital paper demonstrated significant antibacterial activity against *S. aureus*, and the use of titanium dioxide on this type of paper can be particularly attractive and can be an alternative for fighting the proliferation of bacteria, especially in hospital environments. In summary, it was demonstrated that ZnO and TiO_2 nanostructures can be effectively produced with a fast and inexpensive microwave irradiation approach on different cellulose-based substrates creating functionalized papers that can be further adapted and selected to multifunctional applications.

Data Availability

The authors declare that all data supporting the findings of this study are available within the article and its supplementary information files. Nevertheless, if any other information related to the study can be obtained from the corresponding author upon reasonable request.

Conflicts of Interest

The authors declare no competing financial interests.

Acknowledgments

The present research was conducted as part of a master thesis entitled: "Paper-based nanoplatforms for multifunctional applications" by Maria Matias (2018). This work was supported by FEDER funds, through the COMPETE 2020 Program, and national funds, through the Fundação para Ciência e Tecnologia (FCT), under the projects POCI-01-0145-FEDER-007688 (Reference UID/CTM/50025/2019). This work was also supported by FCT/MCTES as the funding entity of MEtRiCS unit under the project UID/EMS/04077/2013. The authors also acknowledge funding from the European Commission through the projects 1D-NEON (H2020-NMP-2015, grant 685758-21D) and BET-EU (H2020-TWINN-2015, grant 692373). The work was also partially funded by the Nanomark collaborative project between INCM (Imprensa Nacional-Casa da Moeda) and CENIMA-T/i3N. D. Nunes and A. Pimentel acknowledge funding from FCT-MCTES through the grants SFRH/BPD/84215/2012 and SFRH/BPD/76992/2011, respectively.

Supplementary Materials

The supplementary information presents the EDS analyses of both pristine paper substrates and the materials after microwave synthesis. The Raman spectroscopy measurements of the ZnO and TiO_2 nanostructures grown on Whatman paper and the paper spectrum itself are also presented together with the XRD measurements of the TiO_2 powder synthesized without the use of any acid during synthesis. Figure S1: SEM images of the pristine papers (a) Whatman, (d) office, and (h) hospital. The corresponding EDS maps of O (b, e, and f), C (c, f, and j), and Ca (g and l). Minimal amounts of Al and Si were detected on hospital paper, appearing as clusters. Table S1: EDS measurements (at.%) of the pristine papers (Whatman, office and hospital), as well as the ZnO nanostructures grown on Whatman paper, TiO_2 grown on hospital paper for 15 min (1 M), and the ZnO/-TiO_2 heterostructure (25 mM-15 min) grown on Whatman paper. Figure S3: Raman spectra of the ZnO and TiO_2 nanostructures grown on Whatman paper under microwave irradiation. The pristine Whatman paper is also presented. Figure S4: XRD measurements of the TiO_2 powder synthesized without the use of any acid during synthesis. *(Supplementary Materials)*

References

[1] A. Pimentel, A. Samouco, D. Nunes, A. Araújo, R. Martins, and E. Fortunato, "Ultra-fast microwave synthesis of ZnO nanorods on cellulose substrates for UV sensor applications," *Materials*, vol. 10, no. 11, pp. 1–18, 2017.

[2] P. F. Carcia, R. S. McLean, M. H. Reilly, and G. Nunes Jr, "Transparent ZnO thin-film transistor fabricated by rf magnetron sputtering," *Applied Physics Letters*, vol. 82, no. 7, pp. 1117–1119, 2003.

[3] I. Repins, M. A. Contreras, B. Egaas et al., "19·9%-efficient ZnO/CdS/CuInGaSe^2 solar cell with 81·2% fill factor," *Progress in Photovoltaics: Research and Applications*, vol. 16, no. 3, pp. 235–239, 2008.

[4] X. Zong and R. Zhu, "ZnO nanorod-based FET biosensor for continuous glucose monitoring," *Sensors and Actuators, B: Chemical.*, vol. 255, pp. 2448–2453, 2018.

[5] K. M. Lee, C. W. Lai, K. S. Ngai, and J. C. Juan, "Recent developments of zinc oxide based photocatalyst in water treatment technology: a review," *Water Research*, vol. 88, pp. 428–448, 2016.

[6] J. O. Carneiro, A. P. Samantilleke, P. Parpot et al., "Visible light induced enhanced photocatalytic degradation of industrial effluents (rhodamine B) in aqueous media using TiO_2 nanoparticles," *Journal of Nanomaterials*, vol. 2016, 13 pages, 2016.

[7] R. Borda d' Água, R. Branquinho, M. P. Duarte et al., "Efficient coverage of ZnO nanoparticles on cotton fibres for antibacterial finishing using a rapid and low cost *in situ* synthesis," *New Journal of Chemistry*, vol. 42, no. 2, pp. 1052–1060, 2018.

[8] P. Dao, *Fabrication and Properties of 1-Dimensional TiO_2 and ZnO Nanocomposites Prepared by Hydrothermal Method*, University College of Southeast Norway, 2016.

[9] V. Coleman and C. Jagadish, "Zinc oxide bulk, thin films and nanostructures : processing, properties and applications," Elsevier Science Ltd., Oxford, 1st edition, 2006.

[10] K. S. Babu, A. R. Reddy, and K. V. Reddy, "Controlling the size and optical properties of ZnO nanoparticles by capping with SiO_2," *Materials Research Bulletin*, vol. 49, pp. 537–543, 2014.

[11] N. Morales-Flores, R. Galeazzi, E. Rosendo, T. Díaz, S. Velumani, and U. Pal, "Morphology control and optical properties of ZnO nanostructures grown by ultrasonic synthesis," *Advances in Nano Research*, vol. 1, no. 1, pp. 59–70, 2013.

[12] D. Nunes, A. Pimentel, A. Araujo et al., "Enhanced UV flexible photodetectors and photocatalysts based on TiO_2 nanoplatforms," *Topics in Catalysis*, vol. 61, no. 15-17, pp. 1591–1606, 2018.

[13] N. G. Park, G. Schlichthörl, J. Van De Lagemaat, H. M. Cheong, A. Mascarenhas, and A. J. Frank, "Dye-sensitized TiO_2 solar cells: structural and photoelectrochemical characterization of nanocrystalline electrodes formed from the hydrolysis of $TiCl_4$," *Journal of Physical Chemistry B*, vol. 103, no. 17, pp. 3308–3314, 1999.

[14] B. O'Regan and M. Grätzel, "A low-cost, high-efficiency solar cell based on dye-sensitized colloidal TiO_2 films," *Nature*, vol. 353, no. 6346, pp. 737–740, 1991.

[15] K. Nakata and A. Fujishima, "TiO_2 photocatalysis: design and applications," *Journal of Photochemistry and Photobiology C: Photochemistry Reviews*, vol. 13, no. 3, pp. 169–189, 2012.

[16] K. Hashimoto, H. Irie, and A. Fujishima, "TiO_2 photocatalysis: a historical overview and future prospects," *Japanese Journal of Applied Physics*, vol. 44, no. 12, pp. 8269–8285, 2005.

[17] J. Schneider, M. Matsuoka, M. Takeuchi et al., "Understanding TiO_2 photocatalysis: mechanisms and materials," *Chemical Reviews*, vol. 114, no. 19, pp. 9919–9986, 2014.

[18] A. Di Paola, M. Bellardita, and L. Palmisano, "Brookite, the least known TiO_2 photocatalyst," *Catalysts*, vol. 3, no. 1, pp. 36–73, 2013.

[19] D. Reyes-Coronado, G. Rodríguez-Gattorno, M. E. Espinosa-Pesqueira, C. Cab, R. De Coss, and G. Oskam, "Phase-pure TiO_2 nanoparticles: anatase, brookite and rutile," *Nanotechnology*, vol. 19, no. 14, pp. 145605–145610, 2008.

[20] L. Gnanasekaran, R. Hemamalini, and K. Ravichandran, "Synthesis and characterization of TiO_2 quantum dots for photocatalytic application," *Journal of Saudi Chemical Society*, vol. 19, no. 5, pp. 589–594, 2015.

[21] A. Jena, R. Vinu, S. A. Shivashankar, and G. Madras, "Microwave assisted synthesis of nanostructured titanium dioxide with high photocatalytic activity," *Industrial and Engineering Chemistry Research*, vol. 49, no. 20, pp. 9636–9643, 2010.

[22] P. Rai and Y. T. Yu, "Citrate-assisted hydrothermal synthesis of single crystalline ZnO nanoparticles for gas sensor application," *Materials Letters*, vol. 173, pp. 58–65, 2012.

[23] N. R. More and U. Chanshetti, "Review article on ZnO thin films by spray pyrolysis review article on ZnO thin films by spray pyrolysis," *International Journal of Chemical and Physical Sciences*, vol. 7, pp. 51–54, 2018.

[24] H. Y. Xu, H. Wang, Y. C. Zhang et al., "Hydrothermal synthesis of zinc oxide powders with controllable morphology," *Ceramics International*, vol. 30, no. 1, pp. 93–97, 2004.

[25] Y. Li, M. Guo, M. Zhang, and X. Wang, "Hydrothermal synthesis and characterization of TiO_2 nanorod arrays on glass substrates," *Materials Research Bulletin*, vol. 44, no. 6, pp. 1232–1237, 2009.

[26] H. Yin, Y. Wada, T. Kitamura et al., "Hydrothermal synthesis of nanosized anatase and rutile TiO_2 using amorphous phase TiO_2," *Journal of Materials Chemistry*, vol. 11, no. 6, pp. 1694–1703, 2001.

[27] B. Liu and H. C. Zeng, "Hydrothermal synthesis of ZnO nanorods in the diameter regime of 50 nm," *Journal of the American Chemical Society*, vol. 125, no. 15, pp. 4430-4431, 2003.

[28] R. J. Barnes, R. Molina, J. Xu, P. J. Dobson, and I. P. Thompson, "Comparison of TiO_2 and ZnO nanoparticles for photocatalytic degradation of methylene blue and the correlated inactivation of gram-positive and gram-negative bacteria," *Journal of Nanoparticle Research*, vol. 15, no. 2, 2013.

[29] R. Goyay and D. Kishore, "Investigation of photocatalytic degradation of rhodamine B by using nano-sized TiO_2," *Journal of Scientific Research and Management*, vol. 5, pp. 6006–6013, 2017.

[30] A. B. Djurišić, Y. H. Leung, and A. M. Ching Ng, "Strategies for improving the efficiency of semiconductor metal oxide photocatalysis," *Materials Horizons*, vol. 1, no. 4, pp. 400–410, 2014.

[31] D. Nunes, A. Pimentel, L. Santos, P. Barquinha, E. Fortunato, and R. Martins, "Photocatalytic TiO_2 nanorod spheres and arrays compatible with flexible applications," *Catalysts*, vol. 7, no. 12, pp. 1–18, 2017.

[32] D. Sharma, S. Sharma, B. S. Kaith, J. Rajput, and M. Kaur, "Synthesis of ZnO nanoparticles using surfactant free in-air and microwave method," *Applied Surface Science*, vol. 257, no. 22, pp. 9661–9672, 2011.

[33] A. ul Hassan Sarwar Rana, M. Kang, and H. S. Kim, "Microwave-assisted facile and ultrafast growth of ZnO nanostructures and proposition of alternative microwave-assisted methods to address growth stoppage," *Scientific Reports*, vol. 6, no. 1, 2016.

[34] P. Sahatiya, A. Kadu, H. Gupta, P. Thanga Gomathi, and S. Badhulika, "Flexible, disposable cellulose-paper-based MoS_2/Cu_2S hybrid for wireless environmental monitoring and multifunctional sensing of chemical stimuli," *ACS Applied Materials & Interfaces*, vol. 10, no. 10, pp. 9048–9059, 2018.

[35] N. A. Ibrahim, B. M. Eid, E. A. El-Aziz, T. M. Abou Elmaaty, and S. M. Ramadan, "Multifunctional cellulose-containing fabrics using modified finishing formulations," *RSC Advances*, vol. 7, no. 53, pp. 33219–33230, 2017.

[36] F. A. Cataño, S. H. Valencia, E. A. Hincapié, G. M. Restrepo, and J. M. Marín, "A comparative study between TiO_2 and ZnO photocatalysis: photocatalytic degradation of cibacron yellow FN-2R dye," *Latin American Applied Research*, vol. 42, no. 1, pp. 33–38, 2012.

[37] R. Fagan, D. E. McCormack, D. D. Dionysiou, and S. C. Pillai, "A review of solar and visible light active TiO_2 photocatalysis for treating bacteria, cyanotoxins and contaminants of emerging concern," *Materials Science in Semiconductor Processing*, vol. 42, pp. 2–14, 2016.

[38] Y. Lan, Y. Lu, and Z. Ren, "Mini review on photocatalysis of titanium dioxide nanoparticles and their solar applications," *Nano Energy*, vol. 2, no. 5, pp. 1031–1045, 2013.

[39] K. Kalyanasundaram, "Photochemical applications of solar energy: photocatalysis and photodecomposition of water," *The Royal Society of Chemistry: Photochemistry*, vol. 41, pp. 182–265, 2013.

[40] M. M. Khan, S. F. Adil, and A. Al-Mayouf, "Metal oxides as photocatalysts," *Journal of Saudi Chemical Society*, vol. 19, no. 5, pp. 462–464, 2015.

[41] B. Liu, Z. Wang, Y. Dong et al., "ZnO-nanoparticle-assembled cloth for flexible photodetectors and recyclable photocatalysts," *Journal of Materials Chemistry*, vol. 22, no. 18, pp. 9379–9384, 2012.

[42] M. Zimbone, M. A. Buccheri, G. Cacciato et al., "Photocatalytical and antibacterial activity of TiO_2 nanoparticles obtained by laser ablation in water," *Applied Catalysis B, Environmental*, vol. 165, pp. 487–494, 2015.

[43] A. Jesline, N. P. John, P. M. Narayanan, C. Vani, and S. Murugan, "Antimicrobial activity of zinc and titanium dioxide nanoparticles against biofilm-producing methicillin-resistant *Staphylococcus aureus*," *Applied Nanoscience*, vol. 5, no. 2, pp. 157–162, 2015.

[44] C. A. Schneider, W. S. Rasband, and K. W. Eliceiri, "NIH image to ImageJ: 25 years of image analysis," *Nature Methods*, vol. 9, no. 7, pp. 671–675, 2012.

[45] R. Borda d'Água, *Desenvolvimento de técnicas de impregnação de nanopartículas de óxido de zinco de baixo custo com propriedades antimicrobianas em tecidos*, FCT, UNL, 2015.

[46] A. C. Alba-Rubio, J. Santamaría-González, J. M. Mérida-Robles et al., "Heterogeneous transesterification processes by using CaO supported on zinc oxide as basic catalysts," *Catalysis Today*, vol. 149, no. 3-4, pp. 281–287, 2010.

[47] H. C. Hsu, C. I. Lin, and H. K. Chen, "Zinc recovery from spent ZnO catalyst by carbon in the presence of calcium carbonate," *Metallurgical and Materials Transactions B: Process Metallurgy and Materials Processing Science*, vol. 35, no. 1, pp. 55–63, 2004.

[48] A. R. Jamaludin, S. R. Kasim, and Z. A. Ahmad, "The effect of $CaCO_3$ addition on physical properties of ZnO-based crystal glaze," *Advanced Materials Research*, vol. 620, pp. 12–16, 2013.

[49] Z. R. Tian, J. A. Voigt, J. Liu, B. Mckenzie, and M. J. Mcdermott, "Biomimetic arrays of oriented helical ZnO nanorods and columns," *Journal of the American Chemical Society*, vol. 124, no. 44, pp. 12954-12955, 2002.

[50] T. Yoshida, "Leaching of zinc oxide in acidic solution," *Materials Transactions*, vol. 44, no. 12, pp. 2489–2493, 2003.

[51] J. Hüpkes, J. I. Owen, S. E. Pust, and E. Bunte, "Chemical etching of zinc oxide for thin-film silicon solar cells," *Chemphyschem*, vol. 13, no. 1, pp. 66–73, 2012.

[52] C. Xu, J. Wang, and Y. Wang, "Synthesis of ZnO nanograins by immersing Zn powders in oxalic acid solution plus thermal decomposition," *Journal of Nanoscience and Nanotechnology*, vol. 15, no. 12, pp. 10002–10007, 2015.

[53] D. Sridev and K. V. Rajendran, "Synthesis and optical characteristics of ZnO nanocrystals," *Bulletin of Materials Science*, vol. 32, no. 2, pp. 165–168, 2009.

[54] V. Causin, C. Marega, A. Marigo, R. Casamassima, G. Peluso, and L. Ripani, "Forensic differentiation of paper by X-ray diffraction and infrared spectroscopy," *Forensic Science International*, vol. 197, no. 1-3, pp. 70–74, 2010.

[55] A. Aminzadeh, "Fluorescence bands in the FT-Raman spectra of some calcium minerals," *Spectrochimica Acta - Part A: Molecular and Biomolecular Spectroscopy*, vol. 53, no. 5, pp. 693–697, 1997.

[56] S. N. White, "Laser Raman spectroscopy as a technique for identification of seafloor hydrothermal and cold seep minerals," *Chemical Geology*, vol. 259, no. 3-4, pp. 240–252, 2009.

[57] M.-C. Chang, P.-I. Liu, L.-C. Chung et al., "A short review: synthesis of anatase TiO_2 and its composite by ionothermal system under microwave heating and their water treatment applications," *Materials Science Research Journal*, vol. 8, pp. 271–292, 2014.

[58] K. Ding, Z. Miao, Z. Liu et al., "Facile synthesis of high quality TiO_2 nanocrystals in ionic liquid via a microwave-assisted process," *Journal of the American Chemical Society*, vol. 129, no. 20, pp. 6362-6363, 2007.

[59] A. V. Murugan, V. Samuel, and V. Ravi, "Synthesis of nanocrystalline anatase TiO_2 by microwave hydrothermal method," *Materials Letters*, vol. 60, no. 4, pp. 479-480, 2006.

[60] A. Fahmi, C. Minot, P. Fourré, and P. Nortier, "A theoretical study of the adsorption of oxalic acid on TiO_2," *Surface Science*, vol. 343, no. 3, pp. 261–272, 1995.

[61] U. Diebold, "The surface science of titanium dioxide," *Surface Science Reports*, vol. 48, no. 5-8, pp. 53–229, 2003.

[62] V. Srikant and D. R. Clarke, "On the optical band gap of zinc oxide," *Journal of Applied Physics*, vol. 83, no. 10, pp. 5447–5451, 1998.

[63] H. Razavi-Khosroshahi, K. Edalati, J. Wu et al., "High-pressure zinc oxide phase as visible-light-active photocatalyst with narrow band gap," *Journal of Materials Chemistry A*, vol. 5, no. 38, pp. 20298–20303, 2017.

[64] T. Luttrell, S. Halpegamage, J. Tao, A. Kramer, E. Sutter, and M. Batzill, "Why is anatase a better photocatalyst than rutile? - model studies on epitaxial TiO_2 films," *Scientific Reports*, vol. 4, no. 1, 2015.

[65] X. Chen, Z. Wu, D. Liu, and Z. Gao, "Preparation of ZnO photocatalyst for the efficient and rapid photocatalytic degradation of azo dyes," *Nanoscale Research Letters*, vol. 12, no. 1, p. 143, 2017.

[66] A. S. Kristoffersen, S. R. Erga, B. Hamre, and Ø. Frette, "Testing fluorescence lifetime standards using two-photon

excitation and time-domain instrumentation: rhodamine B, coumarin 6 and lucifer yellow," *Journal of Fluorescence*, vol. 24, no. 4, pp. 1015–1024, 2014.

[67] F. Chen, J. Zhao, and H. Hidaka, "Highly selective deethylation of rhodamine B: adsorption and photooxidation pathways of the dye on the TiO_2/SiO_2 composite photocatalyst," *International Journal of Photoenergy*, vol. 5, no. 4, p. 217, 2003.

[68] A. A. Al-Kahtani, "Photocatalytic degradation of rhodamine B dye in wastewater using gelatin/CuS/PVA nanocomposites under solar light irradiation," *Journal of Biomaterials and Nanobiotechnology*, vol. 08, no. 01, pp. 66–82, 2017.

[69] S. Xu and Z. L. Wang, "One-dimensional ZnO nanostructures: solution growth and functional properties," *Nano Research*, vol. 4, no. 11, pp. 1013–1098, 2011.

[70] J. Zhang, B. Wu, L. Huang et al., "Anatase nano-TiO_2 with exposed curved surface for high photocatalytic activity," *Journal of Alloys and Compounds*, vol. 661, pp. 441–447, 2016.

[71] W.-Y. Kim, S.-W. Kim, D.-H. Yoo, E. J. Kim, and S. H. Hahn, "Annealing effect of ZnO seed layer on enhancing photocatalytic activity of ZnO/TiO_2 nanostructure," *International Journal of Photoenergy*, vol. 2013, Article ID 130541, 7 pages, 2013.

[72] R. Thapa, S. Maiti, T. H. Rana, U. N. Maiti, and K. K. Chattopadhyay, "Anatase TiO_2 nanoparticles synthesis via simple hydrothermal route: degradation of orange II, methyl orange and rhodamine B," *Journal of Molecular Catalysis A: Chemical*, vol. 363-364, pp. 223–229, 2012.

[73] A. Gustavsson, *Solar Photocatalytic Degradation of Rhodamine B by TiO_2 Nanoparticle Composites*, Doctoral dissertation, Master thesis. University of Gothenburg, Gothenburg, Sweden, 2010.

[74] S. P. Ghosh, K. C. Das, N. Tripathy et al., "Ultraviolet photodetection characteristics of zinc oxide thin films and nanostructures," *IOP Conference Series: Materials Science and Engineering*, vol. 115, 2016.

[75] J. Bai and B. Zhou, "Titanium dioxide nanomaterials for sensor applications," *Chemical Reviews*, vol. 114, no. 19, pp. 10131–10176, 2014.

[76] B. S. Witkowski, L. Wachnicki, S. Gieraltowska et al., "UV detector based on zinc oxide nanorods obtained by the hydrothermal method," *Physica Status Solidi (C)*, vol. 11, no. 9-10, pp. 1447–1451, 2014.

[77] A. Vasudevan, S. Jung, and T. Ji, "On the responsivity of UV detectors based on selectively grown ZnO nanorods," *IEEE Sensors Journal*, vol. 12, no. 5, pp. 1317–1325, 2012.

[78] U. Joost, K. Juganson, M. Visnapuu et al., "Photocatalytic antibacterial activity of nano-TiO_2 (anatase)-based thin films: effects on *Escherichia coli* cells and fatty acids," *Journal of Photochemistry and Photobiology B: Biology*, vol. 142, pp. 178–185, 2015.